www.czasopisma.pan.pl PAN POLSKA AKADEMIA NAUK www.journals.pan.pl

Arch. Min. Sci. **66** (2021), 4, 523-542

Electronic version (in color) of this paper is available: http://mining.archives.pl

DOI: https://doi.org/10.24425/ams.2021.139595

EKIN KÖKEN[1*]

ASSESSMENT OF DEFORMATION PROPERTIES OF COAL MEASURE SANDSTONES THROUGH REGRESSION ANALYSES AND ARTIFICIAL NEURAL NETWORKS

The deformation properties of rocks play a crucial role in handling most geomechanical problems. However, the determination of these properties in laboratory is costly and necessitates special equipment. Therefore, many attempts were made to estimate these properties using different techniques. In this study, various statistical and soft computing methods were employed to predict the tangential Young Modulus (E_{ti}, GPa) and tangential Poisson's Ratio (v_{ti}) of coal measure sandstones located in Zonguldak Hardcoal Basin (*ZHB*), NW Turkey. Predictive models were established based on various regression and artificial neural network (*ANN*) analyses, including physicomechanical, mineralogical, and textural properties of rocks. The analysis results showed that the mineralogical features such as the contents of quartz (Q, %) and lithic fragment (LF, %) and the textural features (i.e., average grain size, d_{50}, and sorting coefficient, S_c) have remarkable impacts on deformation properties of the investigated sandstones. By comparison with these features, the mineralogical effects seem to be more effective in predicting the E_{ti} and v_{ti}. The performance of the established models was assessed using several statistical indicators. The predicted results from the proposed models were compared to one another. It was concluded that the empirical models based on the *ANN* were found to be the most convenient tools for evaluating the deformational properties of the investigated sandstones.

Keywords: Sandstone, Zonguldak, deformation properties, regression analysis, artificial neural network

1. Introduction

Rocks have been used as construction and building material since the dawn of civilisation. Various engineering structures such as bridges, tunnels, and underground caverns have been built in/on rock masses, necessitating detailed investigations on host rock's physicomechanical

[1] ABDULLAH GUL UNIVERSITY, NANOTECHNOLOGY ENGINEERING DEPARTMENT, 38170, KAYSERI, TURKEY

* Corresponding author: ekin.koken@agu.edu.tr

properties, particularly for stability concerns. For the determination of rock properties, the modest method is to obtain core samples. However, high-quality core samples with regular geometry cannot always be extracted from weak, highly fractured, thinly bedded, foliated, and block-in-matrix (*bim*) rocks [1,2]. Besides, in some cases, drilling operations can be challenging in such rock formations associated with underground mines. In these cases, such predictive models help relevant engineers practically analyse their engineering geological problems.

The most commonly measured or estimated mechanical property of rocks is the uniaxial compressive strength (*UCS*, MPa), as it is a consistent relative measure indicating the resistance of rock materials under axial loading conditions. The *UCS* varies remarkably with changing parameters such as lithological variances, rock mineralogy, texture, and degree of weathering [3-13]. Nevertheless, the deformation properties of rocks (i.e., tangential Young Modulus (E_{ti}, GPa) and tangential Poisson's ratio (v_{ti})) are other crucial rock properties in performing numerical modelling of rock masses [14-16]. In terms of underground coal mines, the E_{ti} and v_{ti} have mainly been considered to investigate the strata control issues. They have also been adopted to estimate the stability and fracture evolution of rock mass formations [17-19].

Typical rock types have such specialities that control their behaviour from the point of fracture mechanics. For instance, sandstones including, economic coal and hydrocarbon reserves [20-23], have been mainly identified and investigated using their mineralogical and textural features [24,25]. The degree of breakage in sandstones is controlled by grain size, provenance, maturity, and geological age [26]. When the geological and depositional features are similar in lithofacies, coarser-grained mineral associations cause more fragmentation in sandstones [27]. Retrospectively, earth scientists have long been fascinated by the problem of extracting geologic information from grain-size analyses [26].

As a result, there is immense literature on quantifying the rock texture (*RT*) and rock mineralogy (RM). The *RT* is about variables covering the shape, roundness, size, and fabric of rock-forming minerals. In practical engineering geological approaches, the *RT* is handled by mineral size and distribution of constituents. One of the methods to quantify the *RT* was proposed by Howarth and Rowlands [28]. It was called Texture Coefficient (*TC*) that was correlated with the *UCS* of rocks [8,29,30]. However, the implementation of *TC* is sometimes a challenging issue due to the difficulties in detecting mineral boundaries, distinguishing the matrix or cement from rock-forming minerals, and orientations of grains during thin-section analyses. As another textural feature of rocks, the microfracture density is associated with the weathering degree of rocks [31-33]. In practical approaches, the main conclusion obtained from the RT analyses is that increasing grain size poses heterogeneity and thus decreases the rock strength [34-40]. Although the grain size is a critical phenomenon for the evaluation of rock strength, no direct correlations are obtained between these coupling variables [41].

When it comes to the RM effects on the mechanical properties of rocks, it was determined that increasing quartz content leads to an increase in the *UCS* for several rock types [42,43]. It was noted by Tandon and Gupta [44] that the *UCS* decreases with increasing muscovite content for quartzite rocks. Räisänen M [45] concluded that the abrasion resistance of hybrid granitoids decreases with increasing the heterogeneity in hornblende mineral associations. Cantisani et al. [46] determined that increasing the clay matrix in Italian sandstones poses heterogeneity and has remarkable impacts on the porosity of these rocks. Consequently, researchers have proposed numerous empirical models to predict the mechanical properties of rocks from their physical, mineralogical, petrographical, and other mechanical properties [47-58].

Thanks to these empirical models, practical theories have been postulated, making rock engineering judgments much easier. However, the empirical models to predict dependent variables are primarily unique for any rock type or dataset and are required to be cross-checked by other supportive data and/or quantitative approaches. In this study, several predictive models were proposed to evaluate the E_{ti} and v_{ti} of coal measure sandstones located in the Zonguldak Hardcoal Basin (*ZHB*), NW Turkey. The E_{ti} and v_{ti} were investigated through regression and artificial neural network (*ANN*) methods based on the mineralogical, textural, and physicomechanical properties. The established predictive models were evaluated based on several statistical indicators, and their performances were compared to one another.

2. Materials and methods

Representative rock blocks were obtained from five different underground coal mines located in the ZHB for laboratory studies. A total of 32 different sandstones were investigated in this context. The sampling locations of the rocks are given in Table 1. The mineralogical composition of the sandstones was identified through thin-section and X-ray diffraction (*XRD*) analyses. In thin-section analyses, a polarized microscope (Leica DM750P) was used. The abundance of rock-forming minerals was quantified based on the point-counting method clearly defined by Larrea et al. [59]. Six different images were captured for each thin section scene, considering every 60° of microscope table orientation. From this approach, there were attempts to overcome or minimise the problems arising from optical orientation. A Bruker Discover D8 diffractometer with Cu Kα1 (wavelength 1.54060 Å) radiation source was also utilised in the XRD examinations. These two methods were evaluated together for the determination of sandstone mineralogy. Typical thin sections and *XRD* patterns are shown in Fig. 1.

TABLE 1

Sampling locations of the sandstones

Longwall mine	Depth (m)	Number of rock type
Kozlu	–485 –560	4
Üzülmez	–160 –230	8
Karadon	–360 –460	8
Gelik	–260 –360	7
Amasra	–410 –430	5

As for the textural characterisation, thin sections were digitised using the software ImageJ. The boundaries of grains were filtered thoroughly, and the size and shape properties were determined for each grain. The cementation occupied in thin-section scenes was excluded from the digitisation processes. The particles below 63 μm were also restricted in thin-section analyses; namely, they should be a maximum of 3% of the total number of digitised grains. As a result, the textural characterisation of the sandstones was stated by the average grain size (d_{50}) and sorting coefficient (S_c). The d_{50} and S_c were determined based on the size parameters of the grains. Focusing on the surface area (A_c) and Feret diameters (F_{min}, F_{max}) of each grain, the equivalent diameter (d_e, mm) of a rock-forming mineral was determined by the following equation [60]:

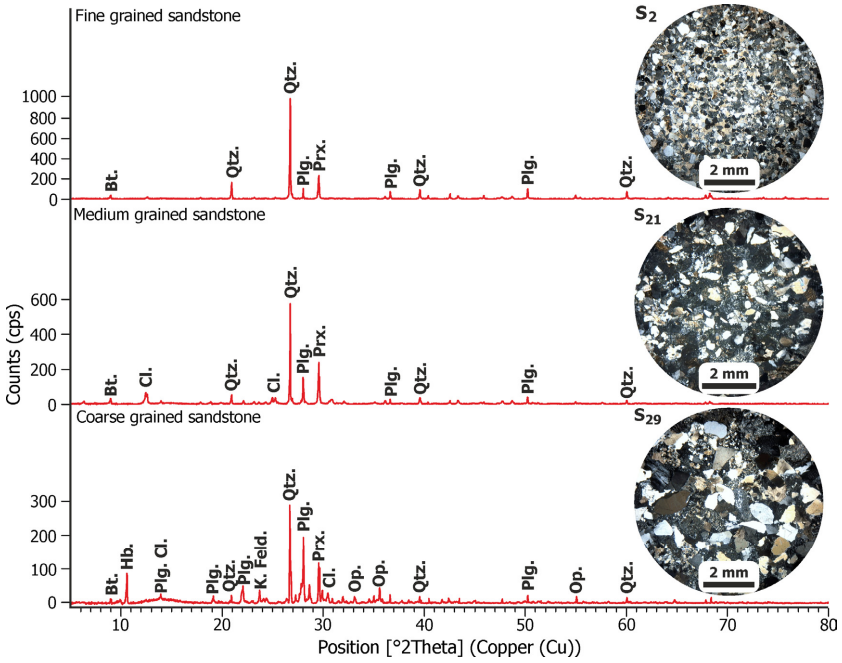

Fig. 1. Typical thin-sections and *XRD* patterns of the sandstones

$$d_e = 0.56\left(A_c\right)^{0.500} + 0.65\left(\frac{\left(F_{\max}F_{\min}\right)^{0.625}}{\left(F_{\max}+F_{\min}\right)^{0.250}}\right) \tag{1}$$

where A_c is the surface area (mm^2), F_{max}, and F_{min} are the maximum and minimum Feret diameters (mm) of the grain, respectively.

Based on d_e values, the S_c was determined using the following equations (Eqs (2) and (3)):

$$\phi = -\log_2(d_e) \tag{2}$$

where ϕ is the size value of the grain and d_e is in mm.

$$S_c = \frac{\phi_{84}-\phi_{16}}{4.0} + \frac{\phi_{95}-\phi_5}{6.6} \tag{3}$$

where ϕ_{95}, ϕ_{84}, ϕ_{16} and ϕ_5 represent the statistical size values corresponding to 95%, 84%, 16%, and 5% of the cumulative density function (*CDF*) of the analysed grains, respectively.

The statistical data were analysed by adopting four different *CDFs*. These were based on the Normal, Gamma, Weibull, and Logistic distributions. Adopting these *CDFs*, four different d_{50} and S_c values were obtained in each textural analysis. The textural characteristics were then conducted by averaging these values for each rock type (Fig. 2).

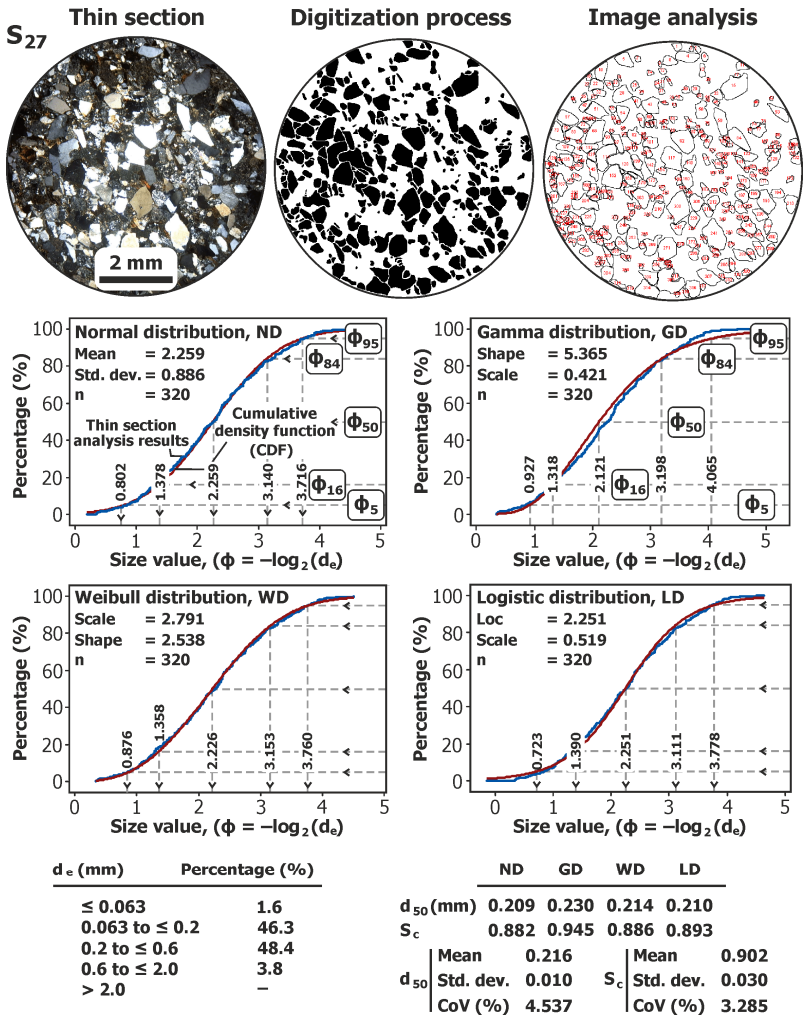

d_e (mm)	Percentage (%)
≤ 0.063	1.6
0.063 to ≤ 0.2	46.3
0.2 to ≤ 0.6	48.4
0.6 to ≤ 2.0	3.8
> 2.0	–

	ND	GD	WD	LD
d_{50} (mm)	0.209	0.230	0.214	0.210
S_c	0.882	0.945	0.886	0.893

d_{50}		S_c	
Mean	0.216	Mean	0.902
Std. dev.	0.010	Std. dev.	0.030
CoV (%)	4.537	CoV (%)	3.285

Fig. 2. Illustration of textural characteristics of the sandstones

3. Laboratory studies

3.1. Mineralogical and textural characteristics

Mineralogical analyses showed that the quartz content (*Q*) varied from 17% to 80%. On the other hand, the ones of Feldspar (*F*) and lithic fragment (*LF*) were found to be between 4-28% and 16-68%, respectively (Table 2). Based on the mineralogical data, the sandstones were identified as lithic arenite and sublitharenite, according to McBride [61] and Dott [62] (Fig. 3a). Furthermore, the sandstones were texturally submature, according to Folk and Ward [63] and Folk [64] (Fig. 3b).

When it comes to variations in grain sizes, the sandstones were divided into three classes in terms of their grain size. Fine-grained ($0.125 \leq d_{50} \leq 0.250$ mm) sandstones were found to be moderately well sorted ($0.5 < S_c \leq 1.0$). Medium ($0.25 < d_{50} \leq 0.50$ mm) and coarse-grained ($0.50 < d_{50} \leq 1.00$ mm) sandstones were poorly and very poorly sorted in some cases. When increasing the grain size, it seems logical to suppose that the S_c values increase in parallel with grain size in the sandstones (Fig 3c). However, the correlation between d_{50} and S_c is not strong ($R^2 = 0.43$).

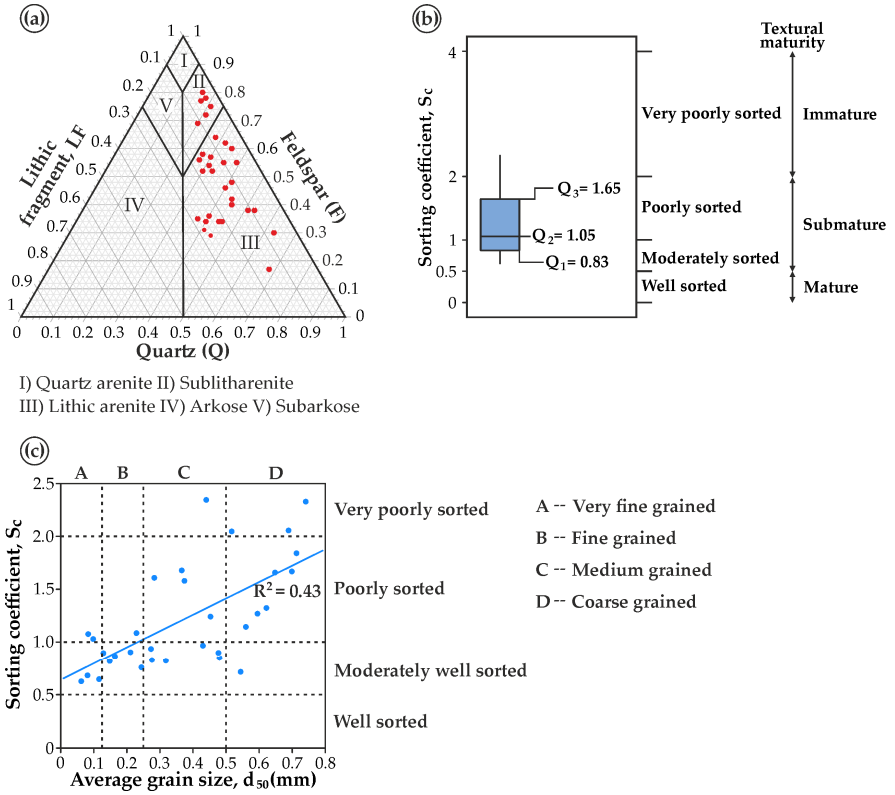

Fig. 3. Mineralogical and textural characterisations of the sandstones: a) Lithofacies classification based on McBride [61] and Dott [62], b) Sorting classification based on Folk and Ward [63] and Folk [64], c) Relationship between d_{50} and S_c

3.2. Physicomechanical properties

Representative rock blocks were drilled using an NX-type core drill for obtaining core samples (Fig. 4a). The core samples were then cut and smoothed following the geometrical conditions of the test instructions. For this purpose, core samples with 54.0 ± 0.2 mm diameter and a length-to-diameter ratio of 2.0-3.0 were prepared for each rock type (Fig. 4b). The physical and mechanical properties were determined in accordance with the methods suggested by the International Society of Rock Mechanics [65]. Effective porosity (n_e, %) and dry unit weight (γ_d, kN/m^3) were determined using a desiccator filled with distilled water at 20 ± 2°C (Fig. 4c).

For the determination of deformation properties (E_{ti}, v_{ti}), linear variable differential transformers (*LVDTs*) were attached to the core samples (Fig. 4d). The pulse wave velocity (V_p, km/s) of the sandstones was also determined using a Pundit Plus ultrasonic testing apparatus (Fig. 4e). For each physicomechanical test on individual sandstones, at least three core samples with proper dimensions were utilised and average values obtained from laboratory studies were presented in Table 2. According to the laboratory test results, the *UCS* ranged from 54 to 166 MPa, while the E_{ti} was between 10 and 34 GPa (Table 2). Considering the *UCS* values in Table 2, the investigated sandstones were identified from moderately hard to hard rock, according to Deere and Miller [66]. Some of the laboratory studies are illustrated in Fig. 4.

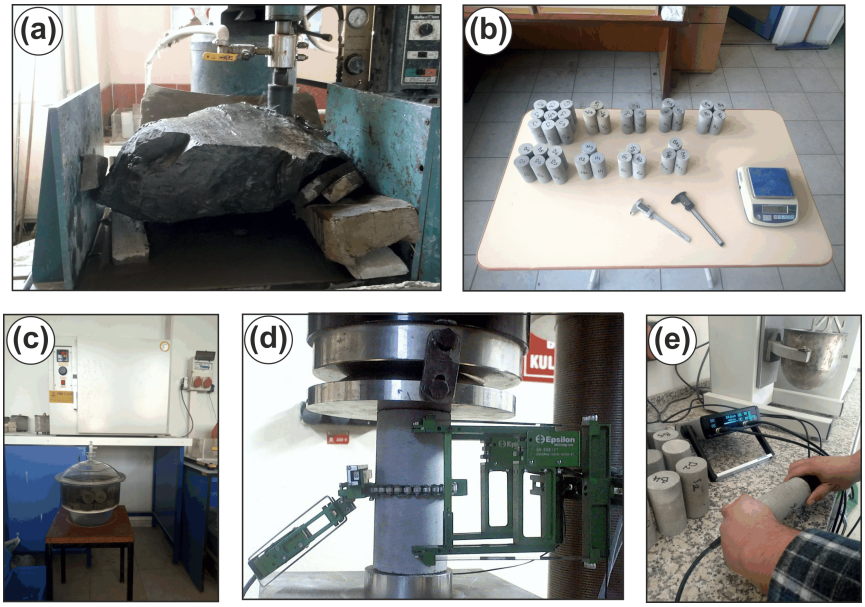

Fig. 4. Laboratory studies: a) Drilling rock blocks, b) Some of the prepared core samples, c) Determination of the n_e and γ_d, d) Determination of the *UCS*, E_{ti} and v_{ti}, e) Pulse wave velocity test

TABLE 2

Laboratory test results

Rock type	γ_d (kN/m^3)	n_e (%)	Q (%)	F (%)	LF (%)	d_{50} (mm)	S_c	UCS (MPa)	V_p (km/s)	v_t (-)	E_{ti} (GPa)
1	2	3	4	5	6	7	8	9	10	11	12
S1	24.82	1.25	52	18	30	0.098	1.029	114.29	4.43	0.15	34.20
S2	25.21	1.27	55	6	39	0.229	1.085	93.13	3.48	0.21	15.77
S3	23.82	5.43	31	28	41	0.713	1.841	79.41	2.71	0.24	16.01
S4	25.20	1.80	57	13	30	0.148	0.815	95.56	3.98	0.21	24.74
S5	24.93	1.72	58	15	27	0.164	0.862	92.17	4.05	0.21	25.40
S6	24.77	2.09	54	15	31	0.129	0.894	87.44	3.22	0.20	21.39
S7	23.85	3.94	36	24	40	0.741	2.329	60.27	2.58	0.25	15.13

TABLE 2. Continued

1	2	3	4	5	6	7	8	9	10	11	12
S8	24.25	4.23	34	26	40	0.595	1.269	58.74	2.54	0.24	13.27
S9	23.84	6.08	48	11	41	0.374	1.580	54.19	2.99	0.28	12.09
S10	24.02	6.47	46	14	40	0.440	2.345	59.28	2.65	0.25	14.80
S11	26.31	1.95	78	4	18	0.318	0.819	115.09	4.15	0.25	25.32
S12	26.63	1.87	80	4	16	0.244	0.755	140.58	4.22	0.22	32.77
S13	26.07	1.68	75	4	21	0.276	0.826	124.16	3.90	0.26	29.92
S14	25.34	1.46	34	22	44	0.366	1.678	92.25	3.50	0.24	18.57
S15	26.65	0.79	69	11	20	0.116	0.644	139.16	4.33	0.16	25.35
S16	26.38	0.86	72	7	21	0.081	0.679	149.74	4.51	0.15	29.11
S17	25.94	1.27	29	27	44	0.430	0.965	100.25	3.00	0.16	15.76
S18	25.32	3.05	40	15	45	0.699	1.668	73.23	2.93	0.19	14.37
S19	25.88	0.71	62	6	32	0.480	0.847	140.60	4.25	0.20	26.87
S20	25.69	3.23	38	11	51	0.453	1.241	95.14	3.51	0.17	20.57
S21	25.70	5.13	42	14	44	0.283	1.608	74.84	3.08	0.22	13.50
S22	25.63	1.90	64	8	28	0.544	0.712	144.50	4.12	0.14	24.10
S23	25.34	1.57	55	10	35	0.273	0.934	105.69	4.05	0.11	20.36
S24	25.47	5.14	60	5	35	0.560	1.144	81.44	3.17	0.22	16.27
S25	24.20	4.65	17	15	68	0.517	2.047	64.80	2.45	0.22	11.16
S26	25.10	0.94	56	17	27	0.083	1.076	106.54	4.27	0.12	32.08
S27	25.31	3.39	30	7	63	0.211	0.902	72.04	2.68	0.19	14.80
S28	25.47	2.56	52	15	33	0.477	0.896	117.80	3.99	0.10	22.10
S29	25.44	2.83	38	9	53	0.648	1.658	87.54	3.39	0.15	19.10
S30	23.80	3.50	35	28	37	0.622	1.323	69.09	2.75	0.27	13.26
S31	23.68	7.86	34	21	45	0.689	2.056	66.53	2.52	0.25	10.52
S32	26.24	0.92	77	6	17	0.062	0.624	166.57	4.62	0.15	29.61

γ_d – Dry unit weight, n_e – Effective porosity, Q – Quartz content, F – Feldspar content, LF – Lithic fragment content, d_{50} – Average grain size, S_c – Sorting coefficient, UCS – Uniaxial compressive strength, V_p – Pulse wave velocity, ν_{ti} – Tangential Poisson's ratio, E_{ti} – Tangential Young modulus

4. Results and discussion

4.1. Prediction models

4.1.1. Regression analyses

The relationships of coupling variables were stated by Pearson's correlation matrix (Table 3). Accordingly, the n_e, Q, LF, S_c, UCS, and V_p are statistically significant, evaluating the E_{ti}. Of these variables, the V_p can be declared a highly correlative parameter, which was also stated by [52,67-71]. On the other hand, the LF and Q as relative indicators of distinguishing sandstone mineralogy seem more influential than textural features on the E_{ti}. This finding is in good agreement with the results of Eberhardt et al. [37] and Sabatakakis et al. [72]. However, Tugrul and Zarif [36] controversially stated that the influence of textural characteristics is more significant than the mineralogical features for granitic rocks.

TABLE 3

Correlation matrix of the variables considered in this study

Variable	γ_d	n_e	Q	F	LF	d_{50}	S_c	UCS	V_p	v_t
n_e	–0.697									
Q	0.668	–0.535								
F	–0.650	0.312	–0.699							
LF	–0.496	0.522	–0.905	0.330						
d_{50}	–0.508	0.601	–0.575	0.436	0.501					
S_c	–0.732	0.760	–0.701	0.500	0.629	0.658				
UCS	0.799	–0.751	0.778	–0.526	–0.715	–0.522	–0.765			
V_p	0.725	–0.788	0.823	–0.546	–0.763	–0.675	–0.773	0.895		
v_t	–0.474	0.559	–0.201	0.207	0.143	0.342	0.486	–0.551	–0.567	
E_{ti}	0.626	**–0.743**	**0.776**	–0.442	**–0.762**	–0.655	**–0.712**	**0.828**	**0.911**	–0.454

Bolded values (e.g.. **0.828**) represent highly correlative ($R \geq 0.70$, $R \leq -0.70$) coupling variables.

In the context of regression analyses, statistically significant relationships are listed in Table 4. It can be claimed that the E_{ti} could be estimated by the regression models (M1-M8). However, the coefficient of determination (R^2) for these models may not be high enough for precise estima-

TABLE 4

Regression analysis results

Empirical formula	Model No	Estimate	Standard error	t value	R^2
$E_{ti} = 27.161n^{-0.365}$	M1	27.161	1.385	19.61	0.56
		–0.365	0.062	5.89	
$E_{ti} = 2.13 + 0.189USC$	M2	2.13	2.39	0.89	0.64
		0.189	0.023	8.21	
$E_{ti} = 35.87 - 1.741n_e - 0.286LF$	M3	35.87	1.99	18.02	0.74
		–1.741	0.403	4.32	
		–0.286	0.061	4.69	
$E_{ti} = 14.20 - 1.683n_e + 0.223Q$	M4	14.20	3.14	4.52	0.75
		–1.683	0.401	4.20	
		0.223	0.046	4.85	
$E_{ti} = -11.11 + 9.052V_p$	M5	–11.11	2.67	–4.16	0.82
		9.052	0.748	12.10	
$E_{ti} = 2.45 + 0.147USC - 3.19\ln(d_{50})$	M6	2.45	2.11	1.16	0.76
		0.147	0.025	5.88	
		–3.19	1.04	3.07	
$E_{ti} = 36.66 - 11.861d_{50} - 0.321LF$	M7	36.66	2.24	16.40	0.68
		–11.86	3.93	–3.02	
		–0.321	0.067	–4.78	
$E_{ti} = 22.187 - 12.88\ln(S_c)$	M8	22.187	0.904	24.54	0.53
		–12.88	2.23	–5.77	
$v_{ti} = 32.296LF^{-0.424}USC^{-0.808}$	M9	32.296	35.465	0.967	0.52
		–0.424	0.131	3.23	
		–0.808	0.144	5.61	

tions. It should also be stated that the lowest R^2 (0.52) was obtained when evaluating the v_{ti} (M9). Therefore soft computing algorithms were attempted to have additional predictive models with higher accuracy, some of which are given in the following sections.

4.1.2. Artificial neural network (*ANN*) applications

The artificial neural network (*ANN*) has been widely adopted to predict several dependent variables based on complex datasets. It is a well-accepted method in most engineering geological problems. In this study, the neural network toolbox (*nntool*) was utilised to establish several neural networks in the MATLAB environment. The dataset was randomly divided into training (70/100) and testing/validating (30/100) parts. Various possible network architectures with variable hidden layers and neurons were attempted to determine the most reliable structural combination. For estimating the E_{ti} and v_{ti}, the most convenient *ANN* architectures were found to be 4–4–1 and 3–6–1, respectively (Fig. 5). To increase training efficiency, the dataset was normalised using the following equation [73,74]:

$$V_N = 2\left(\frac{x_i - x_{\min}}{x_{\max} - x_{\min}}\right) - 1 \tag{4}$$

where x_i is the relevant parameter to be normalised, $x_{\min}$, and $x_{\max}$ are the minimum and maximum values in the dataset (Table 2).

The predicted E_{ti} and v_{ti} values were also denormalised by the following equation:

$$x = 0.5(x_n + 1)(x_{\max} - x_{\min}) + x_{\min} \tag{5}$$

where $x_{\max}$ and $x_{\min}$ values are given in Table 2.

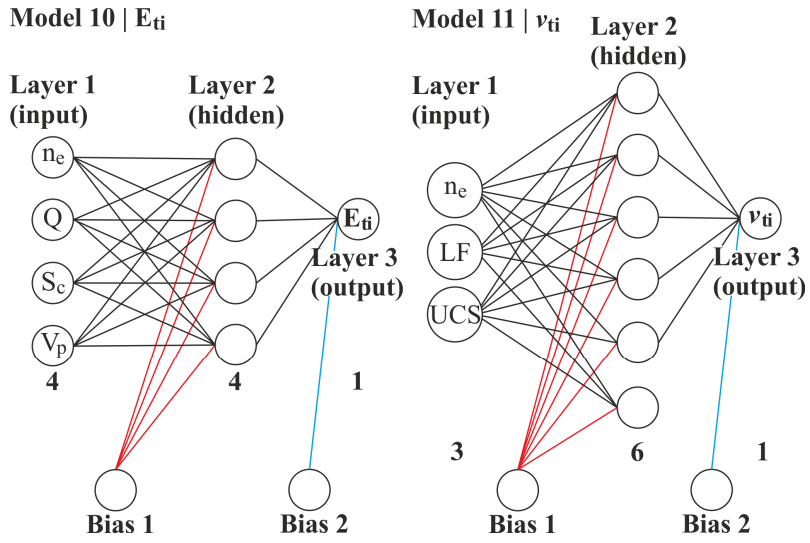

Fig. 5. *ANN* architectures considered in this study

The training of neural networks was conducted using a backpropagation training algorithm with Levenberg-Marquardt training function. Tangent sigmoid (tanh) function was adopted to transmit the data through neurons, which is given by the following equation:

$$\tanh = \frac{2}{1+e^{-2x}} - 1 \tag{6}$$

Different rock properties were adopted in the context of *ANN* analyses (Fig. 5). In light of the above explanations, the *ANN* analyses were carried out with high accuracy. Once the *ANN* has been trained, predictive equations can be established using the weights and biases. In this regard, the empirical models to predict E_{ti} and v_{ti} can be derived from the following equation [74,75]:

$$Y = f_{sig}\left\{b_0 + \sum_{k=1}^{h}\left[w_k \times f_{sig}\left(b_{hk} + \sum_{i=1}^{m} w_{ik} X_{i(N)}\right)\right]\right\} \tag{7}$$

where b_0 is the bias at the output layer, w_k is the connection weight between the kth neuron of the hidden layer and the single output neuron, b_{hk} is the bias at the k^{th} neuron of the hidden layer, h is the number of neurons in the hidden layer, w_{ik} is the connection weight between the i^{th} input variable and k^{th} neuron of the hidden layer, $X_{i(N)}$ is the normalised input variable, f_{sig} is the sigmoid transfer function (i.e., tanh).

Based on the above explanations, the *ANN*-based predictive models are presented in Eq. 8 and Eq. 9. As for the *ANN* analysis results, strong correlations were obtained between the predicted and measured E_{ti} and v_{ti} values (Fig. 6). The coefficients of determination (R^2) for these models were 0.95 and 0.92, respectively. Therefore, the ANN models (M10-M11) have a higher prediction efficiency than the regression models (M1-M9). Mathematical expressions and subfunctions for Eq. 8 and Eq. 9 are also presented in Table 5.

$$E_{ti} = 11.84 \tanh\left(\sum_{i=1}^{4} A_i + 0.7347\right) + 22.36 \tag{8}$$

$$v_{ti} = 0.09 \tanh\left(\sum_{i=1}^{6} A_i + 1.6312\right) + 0.19 \tag{9}$$

where subfunctions (A_i) are given in Table 5.

TABLE 5

Empirical formulae of the proposed ANN models

Model 10 (M10)	**Dependent variable : E_{ti}**
$A_1 = -0.73941 \tanh(-0.31605^n n_e - 1.8092^n Q + 4.4432^n S_c - 0.11964^n V_p + 2.9735)$	
$A_2 = 3.2983 \tanh(-3.2602^n n_e + 0.36492^n Q - 1.0778^n S_c - 4.348^n V_p + 0.55646)$	
$A_3 = -3.0718 \tanh(-3.881^n n_e + 3.8847^n Q - 1.9101^n S_c - 7.1933^n V_p + 0.44225)$	
$A_4 = 1.1302 \tanh(0.013534^n n_e + 2.9422^n Q + 5.9264^n S_c + 5.0804^n V_p - 1.6618)$	

TABLE 5. Continued

Normalization functions for independent variables	
${}^{n}n_e = 0.2797n_e - 1.1986$	${}^{n}Q = 0.0317Q - 1.539$
${}^{n}S_c = 1.1621S_c - 1.7252$	${}^{n}V_p = 0.9217V_p - 3.2581$
Model 11 (M11)	**Dependent variable : v_{ti}**
$A_1 = -1.7392\tanh(-3.7708{}^{n}n_e + 0.85205{}^{n}LF + 1.282{}^{n}UCS + 1.6811)$	
$A_2 = -0.9182\tanh(3.0538{}^{n}n_e + 1.0128{}^{n}LF + 0.041508{}^{n}UCS - 1.3083)$	
$A_3 = 1.7995\tanh(2.1438{}^{n}n_e + 4.9313{}^{n}LF - 4.3467{}^{n}UCS - 0.4404)$	
$A_4 = -2.6048\tanh(4.6183{}^{n}n_e + 3.8207{}^{n}LF + 3.0323{}^{n}UCS + 4.0693)$	
$A_5 = 2.0093\tanh(5.924{}^{n}n_e - 3.4715{}^{n}LF - 0.57324{}^{n}UCS + 2.8373)$	
$A_6 = 2.9519\tanh(-2.7696{}^{n}n_e + 2.5136{}^{n}LF + 0.82155{}^{n}UCS - 1.5425)$	
Normalization functions for independent variables	
${}^{n}n_e = 0.2797n_e - 1.1986$	${}^{n}LF = 0.0385LF - 1.6154$
${}^{n}UCS = 0.0178UCS - 1.9644$	

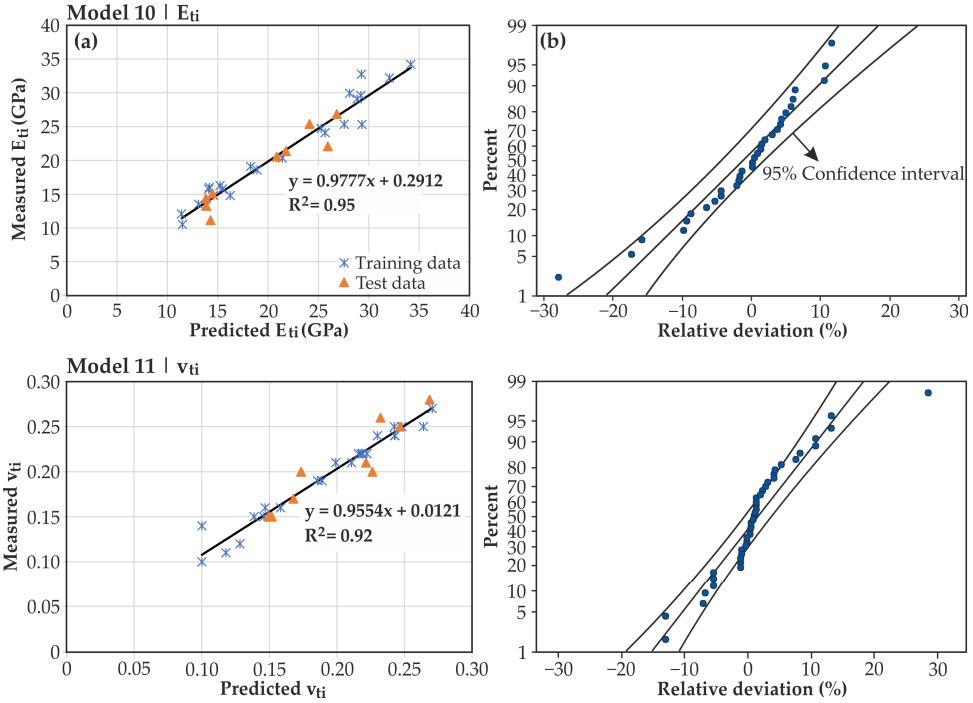

Fig. 6. Correlations obtained from the ANN analyses: a) Predicted and measured values b) Error bands

Several researchers also reported various *ANN* applications to evaluate the E_{ti} for different rock types (Table 6). It is clear from Table 6 that Schmidt hammer rebound value (*SHV*), n_e, and V_p were commonly utilised to predict the E_{ti} in such *ANN* models. In those models,

the ANN architecture of 4–4–1 seems to be much preferable. It should be herein mentioned that the proposed *ANN* models (M10, M11) have several similarities with the models of Heidari et al. [76] and Armaghani et al. [77] in terms of independent variables used and *ANN* architectures adopted.

TABLE 6

Independent variables and used to predict the E_{ti} for various rock types

Rock type	Independent variable	*ANN* architecture	R^2	Reference
Travertine	*SHV*, Is_{50}, V_p, n_e	N.R	0.77	Dehghan et al. [53]
Gypsum	*SHV*, Is_{50}, w_a, V_p	4–9–1	0.89	Yilmaz and Yuksek [68]
Limestone, marl, dolomite	*UCS*, n_e, ρ_d, V_p	4–4–1	0.93	Heidari et al. [76]
Granite	ρ_d, V_p, *Q*, *Plg.*	4–4–1	0.92	Armaghani et al. [77]
Limestone	γ_d, *SHV*, n_e, V_p, I_{d4}	5–2–1	0.71	Yagiz et al. [78]
	E_d, v_d	2–9–1	0.92	Aboutaleb et al. [79]
Sandstone	n_e, V_p, S_c, *Q*	4–4–1	0.95	The present study

N.R – Not reported, *SHV* – Schmidt hammer rebound value, Is_{50} – Point load strength, w_a – water absorption, ρ_d – Dry density, γ_d – Dry unit weight, V_p – Pulse wave velocity, n_e – Effective porosity, *UCS* – Uniaxial compressive strength, I_{d4} – Slake durability index after the fourth cycle, E_d – dynamic Young modulus, v_d – Dynamic Poisson's ratio, *Q* – Quartz content, *Plg* – Plagioclase content, S_c – Sorting coefficient

4.2. Model comparison

Comparing the predictive models was made based on a simple computational code generated in Matlab 2020b, including the empirical formulae established in this study (Table 4, 5). The prediction capability of the models (M1-11) depends on the independent variables considered in the relevant model. Specific to the regression models (M1-M9), it can be claimed that there is no clear superiority over their estimation capability owing to the fluctuation of the predicted results. To prevent overfitting in the estimations, it is recommended to consider all the regression models together. By this comparison, the *ANN*-based models (M10, M11) can be declared the most convenient tools for predicting the E_{ti} and v_{ti} (Fig. 7).

These models are based on n_e, *Q*, *LF*, S_c, V_p, and *UCS* (Fig. 5). The error bands for the *ANN*-based models are almost within the 95% confidence interval limits, which validates their statistical significance (Fig. 6b). The mentioned independent variables for M10, M11, especially mineralogical (*Q*, *LF*), and textural ones (S_c), can be determined from thin-section analyses, previously given in Fig. 1 and 2. In physicomechanical properties, n_e and V_p are nondestructive rock properties, which are easy to handle and easily repeatable [80]. Hence, they can be used to evaluate the E_{ti} of investigated sandstones. When it comes to estimating the v_{ti}, the *LF* and *UCS* were utilised in the models of M9 and M11.

The *LF* for sandstones in the *ZHB* was previously defined as four subgroups. These are gravel substitutions (e.g., micro-quartzite with undulose extinction), detritic igneous constituents (e.h. Hornblende, biotite, tremolite, chlorite, and pyroxene), carbonate fragments (e.g., calcite, aragonite), and opaque minerals (magnetite, rutile etc.) [60]. The more *LF* is, the lower *UCS* values can be expected (Table 3). Owing to this reason, the *LF* was adopted as a reasonable parameter

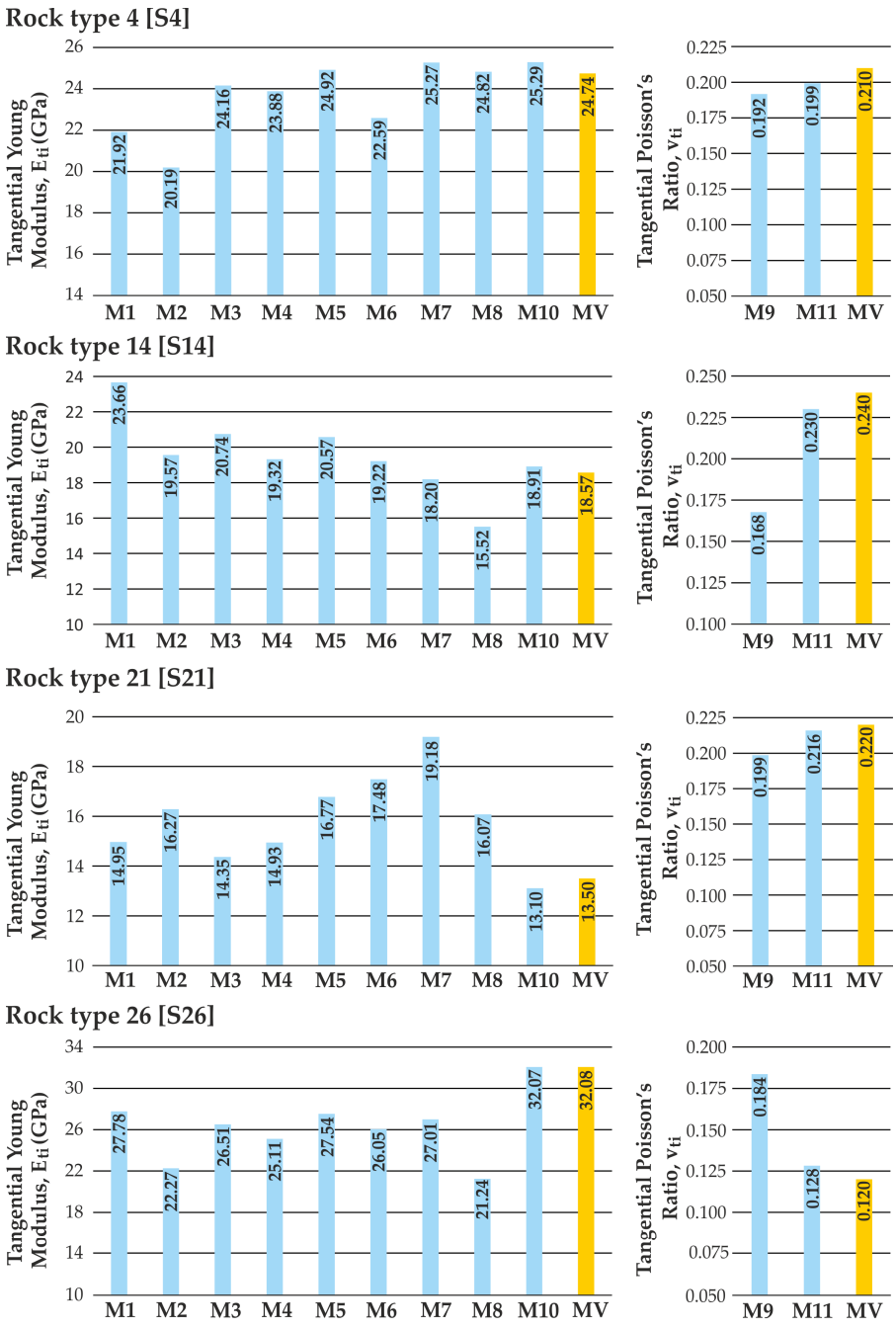

M1–11 : Model 1–11 MV : Measured value

ANN–based models: M10, M11

Fig. 7. Comparison of the predictive models for several sandstones

for predicting the v_{ti}. However, it should be considered thoroughly because of the possibility of subjective mineralogical inferences.

The performance of the proposed models was evaluated using various statistical indices such as root means squared error (*RMSE*), mean-squared-error (*MSE*), mean absolute percentage error (*MAPE*), and the variance accounted for (*VAF*). The equations to calculate the above indices were listed in Eqs. 10-13.

$$RMSE = \sqrt{\frac{\sum_{i=1}^{n}\left(o_i - e_i\right)^2}{n}} \tag{10}$$

$$MSE = \frac{1}{n}\sum_{i=1}^{n}\left(o_i - e_i\right)^2 \tag{11}$$

$$MAPE = \frac{1}{n}\sum_{i=1}^{n}\left|o_i - e_i\right| \tag{12}$$

$$VAF = \left(1 - \frac{\mathrm{var}\left(o_i - e_i\right)}{\mathrm{var}(o_i)}\right) \times 100 \tag{13}$$

where o_i is the observed data, e_i is the estimated data, and n is the number of observations.

The performance evaluation of the models is presented in Table 7. Higher *VAF* and lower *RMSE*, *MSE*, and *MAPE* values indicate relatively more successful models. In this direction, when comparing the regression models with one another, M5 has the lowest relative errors with *RMSE*, *MSE*, and *MAPE* values of 2.82, 7.95, and 2.20, respectively.

TABLE 7

Performance evaluation of the predictive models

Model No	Dependent variable	R^2	*RMSE*	*MSE*	*MAPE*	*VAF*
M1	E_{ti}	0.56	4.53	20.53	3.62	56.13
M2		0.64	3.83	14.72	2.95	68.53
M3		0.74	3.45	11.93	2.72	74.49
M4		0.75	3.40	11.56	2.45	75.28
M5		0.82	2.82	7.95	2.20	82.99
M6		0.76	3.33	11.09	2.67	76.29
M7		0.68	3.86	14.92	3.13	68.11
M8		0.53	4.71	22.19	3.75	52.57
M10[(I)]		0.95	1.58	2.50	1.14	94.70
M9	v_{ti}	0.52	0.03	0.001	0.02	52.47
M11[(I)]		0.92	0.01	0.0002	0.008	93.69

[(I)] ANN-based models

The *VAF* for M5 is 82.99. On the other hand, as tabulated in Table 7, M10 and M11 provide the highest prediction performance among the established models with *VAF* values greater than 93. The performance indices demonstrate that the M10 and M11 can be used to predict the deformation properties of the sandstones when a high degree of accuracy is required. Moreover, regression-based models such as M4 and M5 can also be regarded in conditions where simple estimations of E_{ti} are desired.

5. Conclusion

Predictive models have been established for the evaluation of E_{ti} and v_{ti} in this study. The physicomechanical, mineralogical, and textural properties were determined using 32 different coal-measure sandstones (Table 2). Regression and soft computing analyses were carried out using the laboratory test results. The analysis results demonstrated that the n_e, Q, LF, S_c, UCS, and V_p are statistically significant. Therefore they could be declared correlative parameters for the evaluation of E_{ti}. However, simply no correlative variables are found with regards to the v_{ti}.

Soft computing analyses are carried to fulfil the need for high prediction accuracy. The calculated performance indices have demonstrated that the M10 and M11 could be reliably utilised to estimate the deformation properties of the sandstones (Table 7).

Mining activities in the *ZHB* have been gradually carried out at greater depths that necessitate detailed investigations on coal-measure rocks' physicomechanical properties. Therefore it is logical to suppose that such predictive models based on soft computing tools save time and provide accurate data in rock engineering judgments for roof stability considerations in the *ZHB*. One can claim that the physicomechanical, mineralogical, and textural features of sandstones can reveal the deformational properties when integrated into soft computing algorithms. By changing the independent variables, various *ANN* models can always be welcomed relative to the need. Therefore, there is flexibility in improving the *ANN*-based models by incorporating new test results. The outputs of the experimental studies presented in the paper help provide information on the deformational properties of the investigated sandstones. Nevertheless, further studies are required to obtain such predictive models that consider confining pressures, degree of anisotropy, and predefined cracks.

Declaration of competing interest

The author declares that he has no known competing financial interests or personal relationships that could have influenced the work reported in this paper

References

[1] K. Zorlu, C. Gökçeoglu, F. Ocakoglu, H.A. Nefeslioglu, S. Acikalin, Prediction of uniaxial compressive strength of sandstones using petrography-based models. Eng. Geol. **96**, 141-158 (2008). DOI: https://doi.org/10.1016/j.enggeo.2007.10.009

[2] N. Ceryan, Application of support vector machines and relevance vector machines in predicting uniaxial compressive strength of volcanic rocks. J. African Earth. Sci. **100**, 634-644 (2014). DOI: https://doi.org/10.1016/j.jafrearsci.2014.08.006

[3] A. Shakoor, R.E. Bonelli, Relationship between petrographic characteristics, engineering index properties, and mechanical properties of selected sandstones. Environ. Eng. Geosci. **28**, 55-71 (1991). DOI: https://doi.org/10.2113/gseegeosci.xxviii.1.55

[4] A. Ersoy, M.D. Waller, Textural characterisation of rocks. Eng. Geol. **39**, 123-136 (1995). DOI: https://doi.org/10.1016/0013-7952(95)00005-Z

[5] F.G. Bell, P. Lindsay, The petrographic and geomechanical properties of some sandstones from the Newspaper Member of the Natal Group near Durban, South Africa. Eng. Geol. **53**, 57-81 (1999). DOI: https://doi.org/10.1016/S0013-7952(98)00081-7

[6] R. Prikryl, Assessment of rock geomechanical quality by quantitative rock fabric coefficients: limitations and possible source of misinterpretations. Eng. Geol. **87**, 149-162 2006. DOI: https://doi.org/10.1016/j.enggeo.2006.05.011

[7] J.S. Coggan, D. Stead, J.H. Howe, C.I Faulks, Mineralogical controls on the engineering behavior of hydrothermally altered granites under uniaxial compression. Eng. Geol. **160**, 89-102 (2013). DOI: https://doi.org/10.1016/j.enggeo.2013.04.001

[8] C.A. Ozturk, E. Nasuf, S. Kahraman, Estimation of rock strength from quantitative assessment of rock texture. Journal of the Southern African Institute of Mining and Metallurgy **114** (6), 471-480 (2014).

[9] E. Ali, W. Guang, A. Ibrahim, Microfabrics-Based Approach to Predict Uniaxial Compressive Strength of Selected Amphibolites Schists Using Fuzzy Inference and Linear Multiple Regression Techniques, Environ. Eng. Geosci. **21** (3), 235-245 (2015). DOI: https://doi.org/10.2113/gseegeosci.21.3.235

[10] X.A. Cabria, Effects of weathering in the rock and rock mass properties and the influence of salts in the coastal roadcuts in Saint Vincent and Dominica. Master Thesis, Twente University, (2015).

[11] N.Q.A.M. Yusof, H. Zabidi, Correlation of Mineralogical and Textural Characteristics with Engineering Properties of Granitic Rock from Hulu Langat, Selangor. Procedia Chemistry **19**, 975-980 (2016). DOI: https://doi.org/10.1016/j.proche.2016.03.144

[12] E. Köken A. Özarslan, G. Bacak, Weathering effects on physical properties and material behavior of granodiorite rocks. In: Rock Mechanics and Rock Engineering – From the past to the future Ulusay et al. (Eds), ISRM International Symposium, EUROCK 2016, 331-336 (2016).

[13] T.K. Koca, M.Y. Koca, Classification of weathered andesitic rock materials from the İzmir Subway line on the basis of strength and deformation. Bull. Eng. Geol. Environ. **78**, 3575-3592 (2019). DOI: https://doi.org/10.1007/s10064-018-1346-y

[14] M.N. Bidgoli, Z. Zhao, L. Jing, Numerical evaluation of strength and deformability of fractured rocks. Rock Mech. and Geotech. Eng. **5**, 419-430 (2013). DOI: https://doi.org/10.1016/j.jrmge.2013.09.002

[15] H. Xu, W. Zhou, R. Xie, L. Da, C. Xiao, Y. Shan, H. Zhang, Characterization of Rock Mechanical Properties Using Lab Tests and Numerical Interpretation Model of Well Logs. Math. Prob. Eng. 5967159, (2016). DOI: https://doi.org/10.1155/2016/5967159

[16] J. Shu, L. Jiang, P. Kong, Q. Wang, Numerical Analysis of the Mechanical Behaviors of Various Jointed Rocks under Uniaxial Tension Loading. Appl. Sci. **9**, 1824 (2019). DOI: https://doi.org/10.3390/app9091824

[17] P. Davy, C. Darcel, R. Le Goc, D. Mas Ivars, Elastic Properties of Fractured Rock Masses With Frictional Properties and Power Law Fracture Size Distributions. J. Geophys. Res. **123** (8), 6521-6539 (2018). DOI: https://doi.org/10.1029/2017JB015329

[18] M. Babaeian, M. Ataei, F. Sereshki, F. Sotoudeh, A new framework for evaluation of rock fragmentation in open pit mines. Rock Mech. Geotech. Eng. **11** (2), 325-336 (2019). DOI: https://doi.org/10.1016/j.jrmge.2018.11.006

[19] A.A. Mahmoud, S. Elkatatny, D.A. Shehri, Application of Machine Learning in Evaluation of the Static Young's Modulus for Sandstone Formations. Sustainability **12**, 1880 (2020). DOI: https://doi.org/10.3390/su12051880

[20] D. Lv, Z. Li, J. Chen, H. Liu, J. Guo, L. Shang, Characteristics of the Permian coal-formed gas sandstone reservoirs in Bohai Bay Basin and the adjacent areas. North China, Petrol. Sci. Eng. **78** (2), 516-528, (2011). DOI: https://doi.org/10.1016/j.petrol.2011.06.018

[21] A. Fan, R. Yang, N. Lenhardt, M. Wang, Z. Han, J. Li, Y. Li, Z. Zhao, Cementation and porosity evolution of tight sandstone reservoirs in the Permian Sulige gasfield, Ordos Basin (central China). Marine Petrol. Geol. **103**, 276-293 (2019). DOI: https://doi.org/10.1016/j.marpetgeo.2019.02.010

[22] P. Tan, Y. Jin, L. Yuan, et al., Understanding hydraulic fracture propagation behavior in tight sandstone – coal interbedded formations: an experimental investigation. Pet. Sci. **16**, 148-160 (2019). DOI: https://doi.org/10.1007/s12182-018-0297-z

[23] D.G. Roy, T.N. Singh, Predicting deformational properties of Indian coal: Soft computing and regression analysis approach. Measurement **149**, 106975 (2020). DOI: https://doi.org/10.1016/j.measurement.2019.106975

[24] R. Koch, R. Sobott, Sandsteine: Entstehung, Eigenschaften, Verwitterung, Konservierung, Restaurierung. In: Siegesmund, Snethlage (eds) Schriftenreihe der Deutschen Gesellschaft für Geowissenschaften **59**, 145-174 (2008).

[25] J. Rüdrich, T. Bartelsen, R. Dohrmann, S. Siegesmund, Moisture expansion as a deterioration factor for sandstone used in buildings. Environ. Earth Sci. **63**, 1545-1564 (2010). DOI: https://doi.org/10.1007/s12665-010-0767-0

[26] F.J. Pettijohn, Sand and sandstone, Springer-Verlag Berlin, (1973). e-ISBN: 978-1-4615-9974-6

[27] J.R.L Allen, Petrology, origin and deposition of the highest Lower Old Red sandstone of Shropshire, England. J. Sedimen. Res. **32** (4), 657-697 (1962).

[28] D.F. Howarth, J.C. Rowlands, Quantitative assessment of rock texture and correlation with drillability and strength properties. Rock Mech. Rock Eng. **20**, 57-85 (1987). DOI: https://doi.org/10.1007/BF01019511

[29] A. Azzoni, F. Bailo, E. Rondena, et al., Assessment of texture coefficient for different rock types and correlation with uniaxial compressive strength and rock weathering. Rock. Mech. Rock. Eng. **29**, 39-46 (1996). DOI: https://doi.org/10.1007/BF01019938

[30] M. Alber, S. Kahraman, Predicting the uniaxial compressive strength and elastic modulus of a fault breccia from texture coefficient. Rock Mech. Rock. Eng. **42**, 117-127 (2009). DOI: https://doi.org/10.1007/s00603-008-0167-x

[31] F. Arıkan R. Ulusay, N. Aydın, Characterization of weathered acidic volcanic rocks and a weathering classification based on a rating system. Bull. Eng. Geol. Environ. **66**, 415-430 (2007). DOI: https://doi.org/10.1007/s10064-007-0087-0

[32] Ö. Ündül, A. Tuğrul, On the variations of geoengineering properties of dunites and diorites related to weathering. Environ. Earth Sci. **75**, 1326 (2016). DOI: https://doi.org/10.1007/s12665-016-6152-x

[33] E. Köken, S. Top, A. Özarslan, Assessment of Rock Aggregate Quality Through the Analytic Hierarchy Process (AHP). Geotech. Geol. Eng. **38**, 5075-5096 (2020). DOI: https://doi.org/10.1007/s10706-020-01349-8

[34] R.H.C. Wong, K.T. Chau, P. Wang, Microcracking and grain size effect in Yuen Long Marbles. Int. J. Rock Mech. Min. Sci. Geomech. Abstr. **33** (5), 479-485 (1996). DOI: https://doi.org/10.1016/0148-9062(96)00007-1

[35] Y.H. Hatzor, V. Palchik, The influence of grain size and porosity on crack initiation stress and critical flaw length in dolomites. Int. J .Rock Mech. Min. Sci. **34** (5), 805-816 (1997). DOI: https://doi.org/10.1016/S1365-1609(96)00066-6

[36] A. Tugrul, I.H. Zarif, Correlation of mineralogical and textural characteristics with engineering properties of selected granitic rocks from Turkey. Eng. Geol. **51** (4), 303-317 (1999). DOI: https://doi.org/10.1016/S0013-7952(98)00071-4

[37] E. Eberhardt, B. Stimpson, D. Stead, Effects of grain size on the initiation and propagation thresholds of stress-induced brittle fractures. Rock Mech. Rock Eng. **32**, 81-99 (1999). DOI: https://doi.org/10.1007/s006030050026

[38] R. Přikryl, Some microstructural aspects of strength variation in rocks. Int. J. Rock Mech. Min. Sci. **38** (5), 671-682 (2001). DOI: https://doi.org/10.1016/S1365-1609(01)00031-4

[39] M. Cai, P.K. Kaiser, Y. Tasaka, T. Maejima, H. Morioka, M. Minami, Generalized crack initiation and crack damage stress thresholds of brittle rock masses near underground excavations. Int. J. Rock Mech. Min. Sci. **41** (5), 833-847 (2004). DOI: https://doi.org/10.1016/j.ijrmms.2004.02.001

[40] M. Nicksiar, C.D. Martin, Crack initiation stress in low porosity crystalline and sedimentary rocks. Eng. Geol. **154**, 64-76 (2013). DOI: https://doi.org/10.1016/j.enggeo.2012.12.007

[41] E. Köken, Investigations on Fracture Evolution of Coal Measure Sandstones from Mineralogical and Textural Points of View. Indian Geotech. J. **50**, 1024-1040 (2020). DOI: https://doi.org/10.1007/s40098-020-00427-1

[42] N. Yesiloglu-Gultekin, E.A. Sezer, C. Gokceoglu, H. Bayhan, An application of adaptive neuro fuzzy inference system for estimating the uniaxial compressive strength of certain granitic rocks from their mineral contents. Expert Sys. App. **40** (3), 921-928 (2013). DOI: https://doi.org/10.1016/j.eswa.2012.05.048

[43] N.F. Hassan, O.A. Jimoh, S.A. Shehu, Z. Hareyani, The effect of mineralogical composition on strength and drillability of granitic rocks in Hulu Langat, Selangor Malaysia. Geotech. Geol. Eng. **37**, 5499-5505 (2019). DOI: https://doi.org/10.1007/s10706-019-00995-x

[44] R.S. Tandon, V. Gupta, The control of mineral constituents and textural characteristics on the petrophysical & mechanical (PM) properties of different rocks of the Himalaya. Eng. Geol. **153**, 125-143 (2013). DOI: https://doi.org/10.1016/j.enggeo.2012.11.005

[45] M. Räisänen, Relationships between texture and mechanical properties of hybrid rocks from the Jaala-Iitti complex, southeastern Finland. Eng. Geol. **74**, 197-211 (2004). DOI: https://doi.org/10.1016/j.enggeo.2004.03.009

[46] E. Cantisani, C.A. Garzonio, M. Ricci, S. Vettori, Relationships between the petrographical, physical and mechanical properties of some Italian sandstones. Int. J. Rock Mech. Min. Sci. **60**, 321-332 (2013). DOI: https://doi.org/10.1016/j.ijrmms.2012.12.042

[47] R. Ulusay, K. Tureli, M.H. Ider, Prediction of engineering properties of a selected litharenite sandstone from its petrographic characteristics using correlation and multivariate statistical techniques. Eng. Geol. **38** (1-2), 135-157 (1994). DOI: https://doi.org/10.1016/0013-7952(94)90029-9

[48] S. Kahraman, Evaluation of simple methods for assessing the uniaxial compressive strength of rock. Int. J. Rock Mech. Min. Sci. **38** (7), 981-994 (2001). DOI: https://doi.org/10.1016/S1365-1609(01)00039-9

[49] G.R. Lashkaripour, Predicting mechanical properties of mudrock from index parameters. Bull. Eng. Geol. Environ. **61**, 73-77 (2002). DOI: https://doi.org/10.1007/s100640100116

[50] P.A. Hale, A. Shakoor, A Laboratory Investigation of the Effects of Cyclic Heating and Cooling, Wetting and Drying, and Freezing and Thawing on the Compressive Strength of Selected Sandstones. Environ. Eng. Geosci. **9** (2), 117-130 (2003). DOI: https://doi.org/10.2113/9.2.117

[51] C. Gokceoglu, H. Sonmez, K. Zorlu, Estimating the uniaxial compressive strength of some clay bearing rocks selected from Turkey by nonlinear multivariable regression and rule-based fuzzy models. Expert Systems **26** (2), 176-190 (2009). DOI: https://doi.org/10.1111/j.1468-0394.2009.00475.x

[52] M. Khandelwal, T.H. Singh, Correlating static properties of coal measures rocks with P-wave velocity. Int. J. Coal Geol. **79** (1-2), 55-60, (2009). DOI: https://doi.org/10.1016/j.coal.2009.01.004

[53] S. Dehghan, G.H Sattari, S. Chehreh Chelgani, M.A. Aliabadi, Prediction of uniaxial compressive strength and modulus of elasticity for Travertine samples using regression and artificial neural networks. Min. Sci. Tech. (China), **20** (1), 41-46, (2010). DOI: https://doi.org/10.1016/S1674-5264(09)60158-7

[54] S. Yagiz, Correlation between slake durability and rock properties for some carbonate rocks. Bull. Eng. Geol. Environ. **70** (3), 377-383 (2011). DOI: https://doi.org/10.1007/s10064-010-0317-8

[55] T.N. Singh, A.K. Verma, Comparative analysis of intelligent algorithms to correlate strength and petrographic properties of some schistose rocks. Eng. Comput. **28**, 1-12 (2012). DOI: https://doi.org/10.1007/s00366-011-0210-5

[56] M. Khandelwal, Correlating P-wave velocity with the physicomechanical properties of different rocks. Pure Appl. Geophys. **170**, 507-514 (2013). DOI: https://doi.org/10.1007/s00024-012-0556-7

[57] R. Barzegar, M. Sattarpour, M.R. Nikudel, et al., Comparative evaluation of artificial intelligence models for prediction of uniaxial compressive strength of travertine rocks, Case study: Azarshahr area, NW Iran, Model. Earth Sys. Environ. **2**, 76 (2016). DOI: https://doi.org/10.1007/s40808-016-0132-8

[58] A. Teymen, E.C. Mengüç, Comparative evaluation of different statistical tools for the prediction of uniaxial compressive strength of rocks. Int. J. Min. Sci. Tech. **30** (6), 785-797 (2020). DOI: https://doi.org/10.1016/j.ijmst.2020.06.008

[59] M.L. Larrea, S.M. Castro, E.A. Bjerg, A software solution for point counting. Petrographic thin section analysis as a case study. Arab. J. Geosci. **7**, 2981-2989 (2014). DOI: https://doi.org/10.1007/s12517-013-1032-0

[60] E. Köken, Size Reduction Characterization of Underground Mine Tailings: A Case Study on Sandstones. Nat. Resour. Res. **30**, 867-887 (2021). DOI: https://doi.org/10.1007/s11053-020-09707-2

[61] E.F. McBride, A classification of common sandstones. J. Sediment. Petrol. **33** (3), 664-669, (1963). DOI: https://doi.org/10.1306/74D70EE8-2B21-11D7-8648000102C1865D

[62] R.H. Dott, Wackes, greywacke and matrix: what approach to immature sandstone classification. J. Sedimen. Res. **34**, 625-632 (1964).

[63] R.L. Folk, W.C. Ward, Brazos River bar, a study in the significance of grain size parameters. J. Sedimen. Petrol. **27** (1), 3-26 (1957). DOI: https://doi.org/10.1306/74D70646-2B21-11D7-8648000102C1865D

[64] R.L. Folk, Petrology of sedimentary rocks. Austin: Hemphill Pub. (1981), ISBN: 0-914696-14-9.

[65] ISRM, The complete ISRM suggested methods for rock characterization, testing and monitoring: 1974-2006. In: Ulusay R, Hudson JA (eds) Suggested methods prepared by the commission on testing methods. (2007) International Society for Rock Mechanics (ISRM), (2007), Ankara, Turkey

[66] D.U. Deere, R.P. Miller, Engineering classification and index properties for intact rock. Technical Report Air Force Weapons Laboratory (Report No, AFWL-TR-65-116), 136-184, New Mexico, (1966).

[67] E. Yasar , Y. Erdoğan, Correlating sound velocity with the density, compressive strength and Young's modulus of carbonate rocks. Int. J. Rock Mech Min. Sci. **41**, 871-875 (2004). DOI: https://doi.org/10.1016/j.ijrmms.2004.01.012

[68] I. Yilmaz, G. Yuksek, Prediction of the strength and elasticity modulus of gypsum using multiple regression, ANN and ANFIS models. Int. J. Rock Mech. Min. Sci. **46**, 803-810 (2009).
DOI: https://doi.org/10.1016/j.ijrmms.2008.09.002

[69] Z.A. Moradian, M. Behnia, Predicting the Uniaxial Compressive Strength and Static Young's Modulus of Intact Sedimentary Rocks Using the Ultrasonic Test. Int. J. Geomech. **9** (1), 14-19 (2009).
DOI: https://doi.org/10.1061/(ASCE)1532-3641(2009)9:1(14)

[70] G. Pappalardo, Correlation between P-wave velocity and physical-mechanical properties of intensely jointed dolostones, Peloritani Mounts, NE Sicily. Rock Mech. Rock Eng. **48**, 1711-1721 (2015).
DOI: https://doi.org/10.1007/s00603-014-0607-8

[71] H. Arman, S. Paramban, Correlating natural, dry, and saturated ultrasonic pulse velocities with the mechanical properties of rock for various sample diameters. Appl. Sci. **10**, 9134 (2020).
DOI: https://doi.org/10.3390/app10249134

[72] N. Sabatakakis, G. Koukis, G. Tsiambos, S. Papanakli, Index properties and strength variation controlled by microstructure for sedimentary rocks. Eng. Geol. **97**, 80-90 (2008). DOI: https://doi.org/10.1016/j.enggeo.2007.12.004

[73] R. Singh, A. Kainthola, T.N. Singh, Estimation of elastic constant of rocks using an ANFIS approach, Appl. Soft Comput. J. **12**, 40-45 (2012). DOI: https://doi.org/10.1016/j.asoc.2011.09.010

[74] A.I. Lawal, M.A. Idris, An artificial neural network-based mathematical model for the prediction of blast-induced ground vibrations. Int. J. Environmen. Stud. **77** (2), 318-334, (2020).
DOI: https://doi.org/10.1080/00207233.2019.1662186.

[75] S.K. Das, Artificial neural networks in geotechnical engineering: modeling and application issues, Metaheuristics in water, geotechnical and transport engineering, 231-270 (2013).

[76] M. Heidari, G.R. Khanlari, A.A. Momeni, Prediction of Elastic Modulus of Intact Rocks Using Artificial Neural Networks and non-Linear Regression Methods. Australian J. Basic Appl. Sci. **4** (12), 5869-5879 (2010).

[77] D.J. Armaghani, E.T. Mohamad, E. Momeni, M.S. Narayanasamy, An adaptive neuro-fuzzy inference system for predicting unconfined compressive strength and Young's modulus: a study on Main Range granite. Bull. Eng. Geol. Environ. **74**, 1301-1319 (2015). DOI: https://doi.org/10.1007/s10064-014-0687-4

[78] S. Yagiz, E.A. Sezer, C. Gokceoglu, Artificial neural networks and nonlinear regression techniques to assess the influence of slake durability cycles on the prediction of uniaxial compressive strength and modulus of elasticity for carbonate rocks. Int. J. Numer Anal. Methods Geomech. **36** (14), 1636-1650 (2012).
DOI: https://doi.org/10.1002/nag.1066

[79] S. Aboutaleb, M. Behnia, R. Bagherpour, B. Bluekian, Using non-destructive tests for estimating uniaxial compressive strength and static Young's modulus of carbonate rocks via some modeling techniques. Bull. Eng. Geol. Environ. **77** (4), 1717-1728 (2018). DOI: https://doi.org/10.1007/s10064-017-1043-2

[80] A. Jamshidi, H. Zamanian, R. Zarei Sahamieh, The Effect of Density and Porosity on the Correlation Between Uniaxial Compressive Strength and P-wave Velocity. Rock Mech. Rock Eng. **51**, 1279-1286 (2018).
DOI: https://doi.org/10.1007/s00603-017-1379-8